Title

Mechanism of the Stereoselective α-Alkylation of Aldehydes Driven by the Photochemical Activity of Enamines

Journal

Journal of the American Chemical Society, 138(25)

ISSN

0002-7863

Authors

Bahamonde, Ana
Melchiorre, Paolo

Publication Date

2016-06-29

DOI

10.1021/jacs.6b04871

On the Mechanism of the Stereoselective α-Alkylation of Aldehydes Driven by the Photochemical Activity of Enamines

Ana Bahamonde[†] and Paolo Melchiorre*[,†,‡]

[†]*ICIQ* - Institute of Chemical Research of Catalonia – the Barcelona Institute of Science and Technology, Avinguda Països Catalans 16, 43007 Tarragona, Spain

[‡]*ICREA* - Catalan Institution for Research and Advanced Studies, Passeig Lluís Companys 23, 08010 Barcelona, Spain.

Supporting Information Available

ABSTRACT: Herein we describe our efforts to elucidate the key mechanistic aspects of the previously reported enantioselective photochemical α-alkylation of aldehydes with electron-poor organic halides. The chemistry exploits the potential of chiral enamines, key organocatalytic intermediates in thermal asymmetric processes, to directly participate in the photoexcitation of substrates either by forming a photoactive electron donor-acceptor (EDA) complex or by directly reaching an electronically excited state upon light absorption. These photochemical mechanisms generate radicals from closed-shell precursors under mild conditions. At the same time, the ground state chiral enamines provide effective stereochemical control over the enantioselective radical trapping process. We use a combination of conventional photophysical investigations, nuclear magnetic resonance (NMR) spectroscopy, and kinetic studies to gain a better understanding of the factors governing these enantioselective photochemical processes. Measurements of the quantum yield reveal that a radical chain mechanism is operative, while reaction-profile analysis and rate-order assessment indicate the trapping of the carbon-centered radical by the enamine, to form the carbon-carbon bond, as rate-determining. Our kinetic studies unveil the existence of a delicate interplay between the light-triggered initiation step and the radical chain propagation manifold, both mediated by the chiral enamines.

INTRODUCTION

Ground state enamine chemistry has been extensively explored since the 1950s. Following pioneering studies by Gilbert Stork, organic chemists have exploited enamines' nucleophilic character to trap electrophiles and develop useful two-electron polar processes.[1] Successively, chiral enamines **I**, generated *in situ* upon condensation of aldehydes **1** with secondary amine catalysts, have been recognized as key intermediates of organocatalytic enantioselective reactions (Figure 1a).[2,3] Over the last 15 years, the polar reactivity of enamines has found extensive use for the stereoselective functionalization of carbonyl compounds.[4]

Recently, our research laboratories demonstrated that the synthetic potential of chiral enamines is not limited to the ground state domain, but can be further expanded by exploiting their photochemical activity. We revealed the previously hidden ability of enamines to actively participate in the photoexcitation of substrates and trigger the formation of reactive open-shell species from organic halides.[5] At the same time, ground state chiral enamines can provide effective stereochemical control over the enantioselective radical trapping process. This strategy, where stereoinduction and photoactivation merges in a sole chiral organocatalyst, enables light-driven enantioselective transformations that cannot be realized using the thermal reactivity of enamines. Specifically, we used this approach to develop the α-alkylation of aldehydes[6] with electron-deficient benzyl and phenacyl bromides (Figure 1b)[5a] and bromomalonates (**2c**, Figure 1c).[5c] The reactions were conducted at ambient temperature using household compact fluorescence light (CFL) bulbs as the light source.

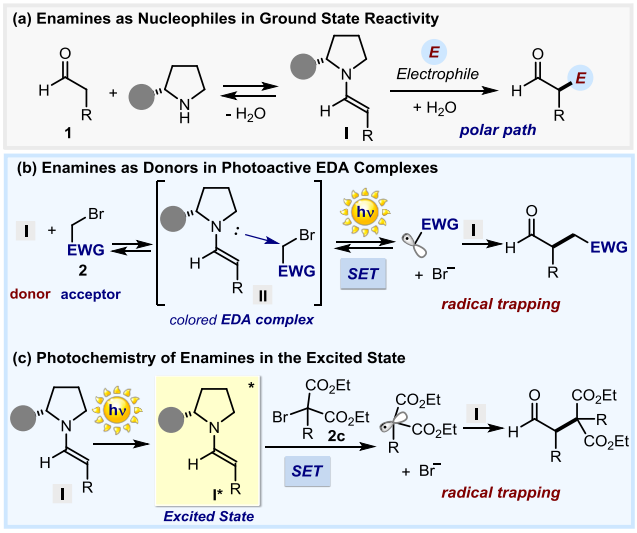

Figure 1. Enamines' reactivity domains. (**a**) *Ground state reactivity*: enamines as nucleophiles in traditional polar processes. *Excited state domain:* enamines can drive the photochemical generation of radicals by (**b**) inducing the formation of ground state, photoactive EDA complexes, and (**c**) acting as a photoinitiator upon direct light excitation. SET = single electron transfer; the grey circle represents the chiral organic catalyst scaffold.

At first glance, both processes depicted in Figure 1b and 1c seem to be classical substitution reactions of enamines proceeding through a S_N2 manifold. However, they do not proceed *at all* without light illumination. Crucial for reactivity was the ability of enamines to trigger the photochemical formation of radicals from the alkyl halides **2** under mild conditions. Despite the superficial similarities between the two chemical transformations, they profoundly diverge in the radical generation mechanism. The first strategy (Figure 1b) relied on the formation of photon-absorbing electron donor-acceptor (EDA) complexes,[7] generated in the ground state upon association of the electron-rich enamine **I** with electron-deficient benzyl and phenacyl bromides. Visible light irradiation of the colored EDA complex **II** induced a single electron transfer (SET), allowing access to the reactive open-shell intermediates. In the second approach (Figure 1c), we used the capability of the chiral enamine **I** to directly reach an electronically excited state (**I***) upon light absorption and then to act as effective photoinitiator. SET reduction of the bromomalonate **2c** induced the formation of the carbon-centered radical.

In this paper, we detail how a combination of conventional photophysical investigations, nuclear magnetic resonance (NMR) spectroscopy, kinetic studies, and quantum yield measurements revealed further mechanistic analogies and striking differences for these enamine-mediated photochemical enantioselective alkylations of aldehydes with electron-poor alkyl halides. From a broader perspective, these studies explain how it is possible to translate the effective tools governing the success of ground state asymmetric enamine catalysis into the realm of photochemical reactivity,[8] thus providing novel reactivity frameworks for conceiving light-driven enantioselective catalytic processes.[9]

RESULTS and DISCUSSION

Our recent studies[5] established that enamines **I** can interact with visible light in two different ways, serving either as donors in photoactive EDA complex formation (Figure 1b) or as photoinitiators upon direct excitation (Figure 1c). As the prototypical reactions for mechanistic analysis, we selected the alkylations of butanal (**1a**) with 2,4-dinitrobenzyl bromide (**2a**, Figure 2a), phenacyl bromide (**2b**, Figure 2b), and diethyl bromomalonate (**2c**, Figure 2c), all promoted by the commercially available diarylprolinol silyl ether catalyst **A**[10] (20 mol%).[11] The reactions with **2a** and **2b** are representative of the EDA complex activation strategy,[5a,b] while the chemistry in Figure 2c is triggered by the direct photoexcitation of the enamine.[5c] For all the processes, and in accordance with the original reports, we confirmed that irradiation by a household 23 W CFL bulb was needed to achieve the alkylation products **3a-3c** in high yield and enantioselectivity.[12] The careful exclusion of light completely suppressed the reactions, confirming their photochemical nature. The inhibition of the reactivity was also observed under an aerobic atmosphere or in the presence of TEMPO (1 equiv), the latter experiment indicating a radical mechanism. Along with these similarities, the light-triggered reactions in Figure 2 showed striking differences too. When the experiments were conducted under illumination by a 300 W Xenon lamp equipped with a cut-off filter at 385 nm and a band-pass filter at 400 nm (irradiation at $\lambda \geq 385$ nm and $\lambda = 400$ nm, respectively), the reactivity of the three processes remained unaltered. However, the use of a band-pass filter at 450 nm or a blue LED (λ_{max} at 450 nm) completely inhibited the reaction with diethyl bromomalonate **2c**. In sharp contrast, the enamine-mediated alkylations with **2a** and **2b** were not affected. We decided to conduct spectroscopic investigations to rationalize the different light-wavelength/reactivity correlation profiles while elucidating the origins of the enamine's photochemical activity.

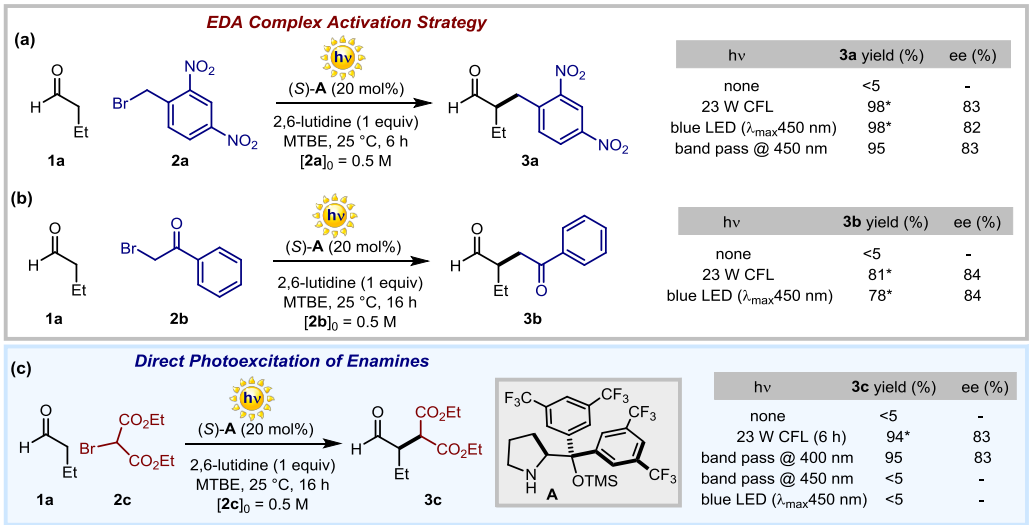

Figure 2. The model photochemical alkylations of butanal **1a** catalyzed by the chiral secondary amine **A**: the enamine-based EDA complex activation in the reaction of (**a**) 2,4-dinitrobenzyl bromide **2a**, and (**b**) phenacyl bromide **2b**; (c) the direct photoexcitation of enamines in the alkylation of **1a** with diethyl bromomalonate **2c**; MTBE: methyl *tert*-butyl ether. NMR yield of **3** determined by ^{1}H NMR spectroscopic analysis of the crude reaction mixture using 1,1,2-trichloroethene as the internal standard.*Yield of the isolated products **3**.

Spectroscopic Studies. Making observations is the basis of the scientific method. In organic chemistry, observing the physical aspects of a reaction may be critical for developing a new methodology or acquiring mechanistic insights. This was certainly true for the enamine-mediated photochemical α-alkylation of aldehydes that we developed. Immediately after mixing an MTBE solution of the enamine, generated *in situ* upon condensation of butanal **1a** (3 equiv) with 20 mol% of catalyst **A**, with 2,4-dinitrobenzyl bromide **2a** (1 equiv), we observed that the achromatic solution turned to a marked yellow color (Figure 3a). This observation raised the question of how the color developed.

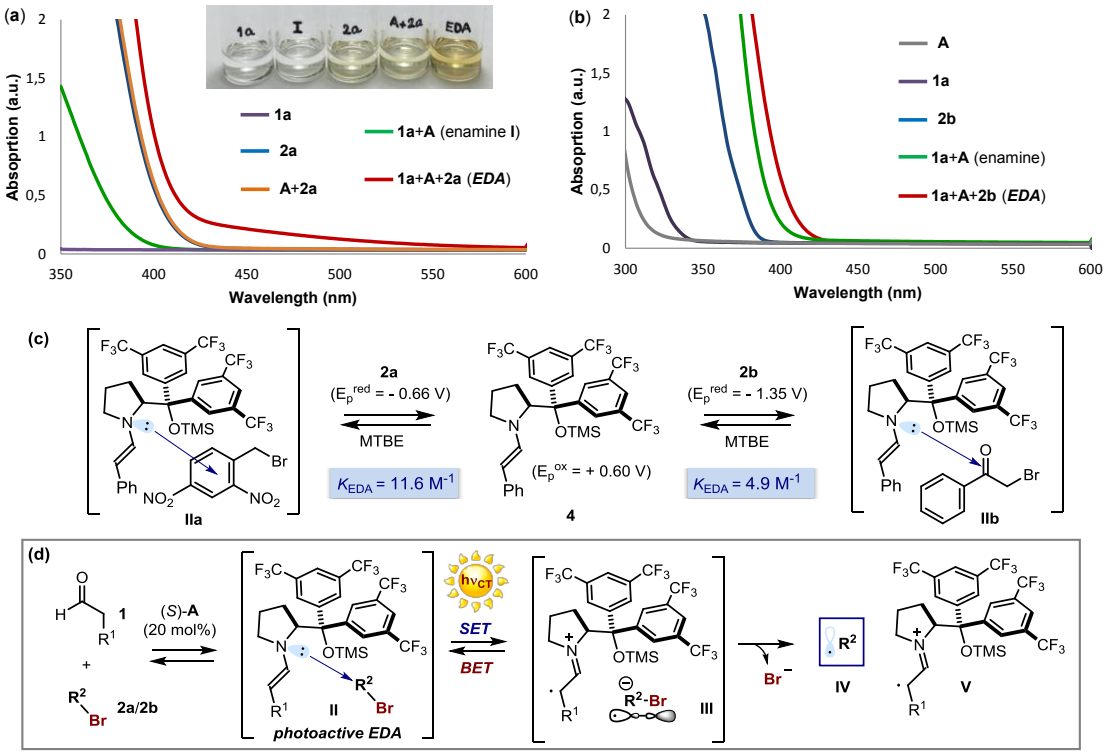

Figure 3. (**a**) Optical absorption spectra, recorded in MTBE in 1 mm path quartz cuvettes using a Shimadzu 2401PC UV-visible spectrophotometer, and visual appearance of the separate reaction components and of the colored EDA complex in the alkylation of 2,4-dinitrobenzyl bromide **2a**; [**1a**] = 1.5 M; [**2a**] = 0.5 M; [**A**] = 0.1 M. (**b**) Optical absorption spectra in MTBE for the alkylation with phenacyl bromide **2b**; [**1a**] = 1.5 M; [**2b**] = [**A**] = 0.2 M. (**c**) Investigating the formation of the EDA complexes in MTBE using the preformed enamine **4**; K_{EDA} is the association constant for the EDA complex formation; E_p^{red} for **2a** and **2b** (irreversible reduction) and E_p^{ox} for **4** (irreversible oxidation) measured by cyclic voltammetry *vs* Ag/Ag^+ in CH_3CN. (**d**) The visible-light-triggered generation of the electrophilic carbon-centered radical **IV** and the α-iminyl radical cation **V** using the enamine-based EDA complex strategy; $h\nu_{CT}$ = charge-transfer transition energy;[15] BET = back electron transfer.

The appearance of strong color on bringing together two colorless organic compounds is not uncommon. In 1952, this phenomenon inspired Robert Mulliken to formulate the charge-transfer theory.[7c] According to this theory, the association of an electron-rich substrate with a low ionization potential (such as an enamine)[13] with an electron-accepting molecule with a high electronic affinity[14] (such as electron-deficient benzyl and phenacyl bromides) can bring about the formation of a new molecular aggregation in the ground state: the electron donor-acceptor complex. EDA complexes are characterized by physical properties that differ from those of the separated substrates. This is because new molecular orbitals form, emerging from the electronic coupling of the donor and acceptor frontier orbitals (HOMO/LUMO). EDA formation is accompanied by the appearance of a new absorption band, the charge-transfer band ($h\nu_{CT}$), associated with an intracomplex transfer of a single electron (SET) from the donor to the acceptor. In many cases, the energy of this transition lies within the visible range.[15] This is what happened when mixing together the enamine, generated *in situ* upon condensation of catalyst **A** and **1a**, with both 2,4-dinitrobenzyl bromide **2a** (E_p^{red} = -0.66 V *vs* Ag/Ag^+ in CH_3CN) and phenacyl bromide **2b** (E_p^{red} = -1.35 V *vs* Ag/Ag^+ in CH_3CN). Indeed, the optical absorption spectra showed a bathochromic displacement in the visible spectral region, where none of the substrates absorbs (red lines, Figures 3a and 3b). The new absorption bands, which in the case of **2a** can reach the green region of the visible range (550 nm), cannot be accounted for by the addition of the absorption of the separate compounds, which can barely absorb visible light.

To further examine the implication of the enamine in the formation of photoactive EDA complexes, we synthesized the enamine **4** (E_p^{ox} = +0.60 V *vs* Ag/Ag^+ in CH_3CN), prepared by condensation of catalyst **A** and 2-phenylacetaldehyde[16] in the presence of molecular sieves. Upon isolation, **4** was mixed with electron acceptors **2a** and **2b** (Figure 3c). Using Job's method[17] of continuous variations, we readily established a

molar donor/acceptor ratio of 1:1 in solution for both colored EDA complexes **IIa** and **IIb,** respectively (details in Section D of the Supporting Information, SI). Concomitantly, an association constant (K_{EDA}) of 11.56 ± 0.02 M^{-1} for the complex **IIa** and 4.9 ± 0.1 M^{-1} for **IIb** in MTBE was determined by spectrophotometric analysis using the Benesi-Hildebrand method.[18]

The light-wavelength /reactivity correlation for the photochemical alkylations of butanal with **2a** and **2b** (Figures 2a and 2b, respectively) can be rationalized on the basis of the photoactivity of the enamine-based EDA complexes **IIa** and **IIb** (their absorption spectra, which are similar to the EDA absorption in Figures 3a and 3b, are reported in Figure S6 within the SI). Absorption of low-energy photons, including visible light, can induce an electron transfer to occur, leading to the chiral ion pair **III** (Figure 3d). Critical to reaction development is the presence of the bromide anion within the radical anion partner in **III**. The bromide, acting as a suitable leaving group, triggers an *irreversible* fragmentation event[19] rapid enough to compete with a possible back electron transfer (BET), which would unproductively restore the ground state EDA complex **II** instead.[20] This fragmentation productively renders two reactive radical intermediates (the electrophilic carbon-centered radical **IV** and the α-iminyl radical cation **V**) which can initiate synthetically useful transformations, i.e. the alkylation of aldehydes. The enamine-based EDA complex activation strategy thus provides ready access to open-shell reactive species under very mild conditions and without the need for any external photoredox catalyst.

The enantioselective photochemical alkylation of butanal **1a** with diethyl bromomalonate **2c** showed profoundly different behavior. In addition to the distinct effect the light frequency had on the reactivity (as discussed in Figure 2), we did not observe any color change in the solution, which remained achromatic during the reaction progression. The absence of any photoabsorbing ground state EDA complex was further confirmed by the optical absorption spectrum of the reaction mixture (red line in Figure 4), which perfectly overlaid the absorption of the enamine, generated upon condensation of the catalyst **A** with **1a** (green line in Figure 4). In a separate experiment, we observed that the addition of a large excess of **2c** to a solution of enamines did not change the absorption spectra, further excluding any EDA association in the ground state (Figure S13 in the SI). Closer inspection of the absorption spectrum indicated that the only photoabsorbing compound at 400 nm (a wavelength suitable for triggering the reaction) was the enamine[21] (green line in Figure 4, absorption band till 415 nm). This observation prompted us to evaluate the possibility that the direct photoexcitation of the enamine could trigger the radical generation from **2c**. This mechanistic scenario was consonant with the experiment performed using a band-pass filter at 450 nm (a wavelength that could not be absorbed by the enamine), since a complete inhibition of the reaction was observed (Figure 2c). The implication of the enamine within the photochemical regime was unambiguously established by Stern-Volmer quenching studies. As detailed in our original study,[5c] we recorded the emission spectra of enamine **4** upon excitation at 365 nm. The excited state of **4** and its emission were effectively quenched by bromomalonate **2c** (see Section E2 in the SI for details).

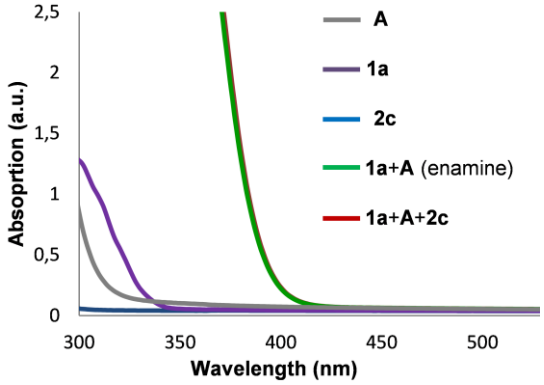

Figure 4. Optical absorption spectra acquired in MTBE in 1 cm path quartz cuvettes; [**1a**] = 1.5 M; [**2c**] = 0.5 M; [**A**] = 0.1 M.

These observations indicate that the photochemical activity of chiral enamines and their potential for light-induced radical generation is not limited to the formation of ground state EDA complexes. As detailed in Figure 5, the enamine **I**, upon light absorption, can reach an electronically excited state (**I***) and act as a photoinitiator, triggering the formation of the electron-deficient radical **IVc** through the reductive cleavage of the bromomalonate C–Br bond via a SET mechanism[22] (E_p^{red} of **2c** = -1.69 V *vs* Ag/Ag^+ in CH_3CN). The reduction potential of the excited enamine was estimated as <-2.0 V (vs Ag/Ag^+ in CH_3CN) on the basis of electrochemical and spectroscopic measurements (see Section E3 in the SI for details).[23] In analogy with the EDA complex activation (Figure 3d), here too the SET event leads to both an electrophilic radical **IV** and the α-iminyl radical cation **V**.

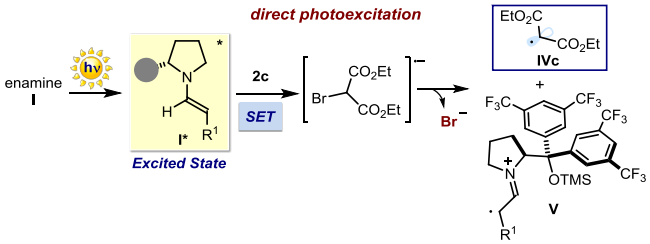

Figure 5. Radical generation strategy based on the direct photoexcitation of the chiral enamine **I**; the grey circle represents the chiral organic catalyst scaffold.

Quantum Yield Measurements and the Proposed Mechanisms. Photophysical investigations established that *in situ* generated chiral enamines can use two different photochemical mechanisms to provide open-shell species from organic halides **2a-c** while avoiding the need for any external photoredox catalyst. We then focused on the non-photochemical steps inherent to the enantioselective alkylation of butanal **1a**. As depicted in Figures 3d and 5, the enamine-mediated photochemical pathways bring about the formation of two radical species: the chiral radical cation **V** and the electrophilic radicals **IV**. A stereocontrolled radical-radical coupling of **IV** and **V** can be invoked to account for the formation of the new carbon-carbon bond and the α-carbonyl stereogenic center within the final products **3a-c** (Figure 6a). This mechanistic frame-

work would require an enamine-mediated photochemical event for every molecule of product generated.

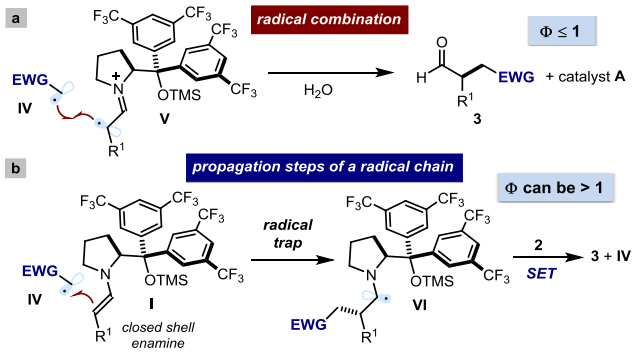

Figure 6. Possible pathways for the non-photochemical steps of the model reactions: (**a**) in-cage radical-radical coupling, and (**b**) radical chain propagation manifold. The open-shell intermediates **V** and **IV** are generated through the photochemical activity of the enamines, as detailed in Figures 3d and 5. EWG: electron-withdrawing group. Φ = quantum yield; see Ref. 27 for an explanation of the quantum yield values.

It must be noted, however, that many radical reactions generally proceed through self-propagating radical-chain pathways.[24] In chain processes, product formation occurs through propagation steps that convert the open-shell intermediate (originating from the substrate precursor) into the final product while regenerating the chain-propagating radical. Reactions will occur if the propagation sequence is rapid enough in comparison with possible termination pathways, and if there is a suitable mode of initiation (that is, effective radical formation from a closed-shell substrate). In our case (Figure 6b), a chain propagation sequence can be envisaged such that the nucleophilic ground state enamine **I** would trap the photochemically-generated electrophilic radical **IV** to form the α-amino radical **VI**. Since α-aminoalkyl radicals are known to be strong reducing agents,[25] **VI** would induce the reductive cleavage of the electron-poor alkyl bromide **2** through an outer-sphere SET process, thereby regenerating the radical **IV** while releasing the product **3** and the aminocatalyst **A** (more mechanistic details are discussed in Figure 7). In this scenario, the enamine-based photochemical radical generation strategies, which afford radicals **IV** and **V**, would serve only to initiate a radical self-propagating chain process.

To help distinguish between the two mechanisms, we determined the quantum yield (Φ)[26] of the model reactions, which defines the moles of product formed per moles of photons absorbed by the system.[27] Using potassium ferrioxalate as the actinometer, we determined quantum yields of 25, 20, and 20 for the reactions in CH_3CN[28] with **2a**, **2b**, and **2c**,[29] respectively (λ = 450 nm for **2a-b** and 400 nm for **2c**). These results are consonant with a self-propagating radical chain mechanism as the main reaction pathways for the three enamine-mediated photochemical alkylations of butanal under study.

Figure 7 details the general mechanism proposed for the alkylation of butanal with 2,4-dinitrobenzyl bromide **2a**, phenacyl bromide **2b**, and diethyl bromomalonate **2c**. They differ in the nature of the light-triggered initiation step, but are characterized by a similar propagation cycle in which the ground state enamine **I** traps the photogenerated electrophilic radical **IV**.

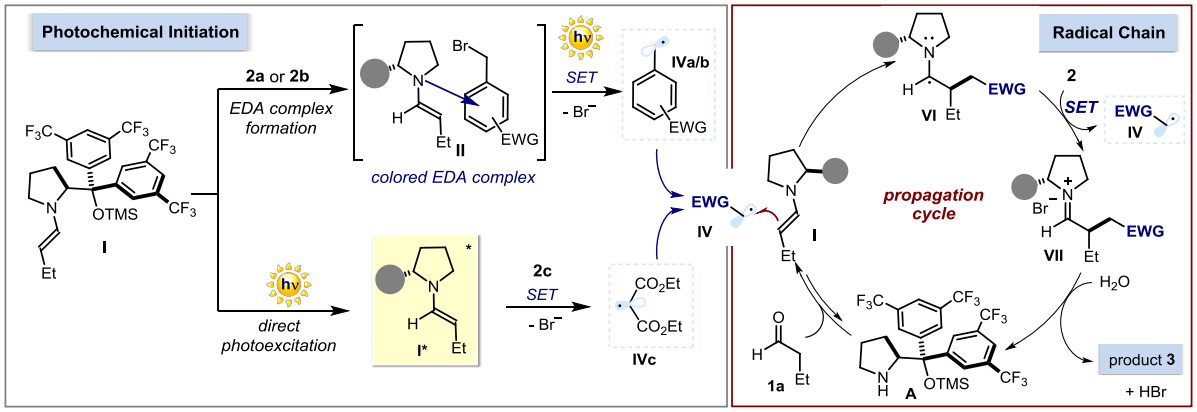

Figure 7. The chain propagation manifold underlying the mechanism of the photochemical enamine-mediated enantioselective α-alkylation of butanal. The initiation event, which generates the electrophilic radicals **IV**, is driven by the photochemical activity of the enamines (EDA complex formation or direct photoexcitation), while the propagation sequence is triggered by the radical trapping by the enamine **I** and the SET reduction of the organic halide **2** from the the α-amino radical **VI**, which acts as a reducing agent. The grey circle represents the chiral scaffold of the organic catalyst **A**.

Overall, the mechanism exploits the dichotomous reactivity profile of enamines in the ground and excited states. The photochemical activity of the enamines, either by EDA complex activation or direct excitation, generates radicals **IV** from the closed-shell intermediates **2a-c** (Figure 7, left panel).[30] This event, by feeding in radicals from outside the chain, serves as the initiation of self-propagating radical chains. The propagation cycle initiates with the radical trap from the ground state chiral enamine **I** (Figure 7, right panel). Considering the consolidated ability of catalyst **A** to infer high stereoselectivity in enamine-mediated polar reactions,[10] it is no surprise that the addition of the radical **IV** to **I** proceeds in a stereocontrolled fashion. The resulting α-aminoalkyl radicals **VI** can then transfer an electron to the starting alkyl halides **2**. This SET process

regenerates the chain-propagating radical **IV** while giving the bromide-iminium ion pair **VII**, which eventually hydrolyzes to release the product **3** and the aminocatalyst **A**. The outer-sphere SET process, a crucial propagation step, is facilitated by the formation of the stable bromide and iminium ions. Notably, in the case of bromomalonate **2c**, an alternative atom-transfer mechanism can be envisaged, where the α-aminoalkyl radical **VI** would abstract a bromine atom from **2c**, regenerating the radical **IV** while affording an unstable α-bromo amine adduct,[31] which would eventually evolve to the iminium ion pair **VII**.

Several aspects of the mechanism proposed in Figure 7 deserve comment. The underlying radical chain pathway is not surprising when considering that the transformation closely resembles a Kornblum-Russell $S_{RN}1$-type alkylation.[32] The $S_{RN}1$ is a process through which nucleophilic substitution is achieved on aromatic and aliphatic compounds that bear a suitable leaving group and that do not react through polar nucleophilic mechanisms. This class of transformations is characterized by an innate chain mechanism involving electron transfer steps with radical ions as intermediates. In some example of $S_{RN}1$-type reactions, electron rich olefins, including enamines,[33] efficiently trap electrophilic radicals. In addition, electron-poor benzyl[33] and phenacyl[34] bromides are suitable substrates for the $S_{RN}1$ reaction manifold.

Another aspect to consider is the central role of the chiral aminocatalyst **A**. Although the process is characterized by an innate radical chain, the organic catalyst plays a direct role in product formation. Indeed, **A** is essential for the propagation mechanism since it transforms an inactive substrate (the aldehyde **1**), which is unsuitable for participating in the radical chain, into the electron-rich chiral enamine **I**, a key intermediate of the propagation cycle. In addition, the enamine is directly involved in both the stereo-defining event and the photochemical initiation. As for the initiation, the fate of the chiral α-iminyl radical cation **V**, emerging from the photoinduced SET to **2** (Figures 3d and 5), deserves further comment. Intermediate **V** is an unproductive species, since it lies outside of the chain propagation manifold which converts substrates into products. We have obtained evidence that **V** is an unstable intermediate which cannot be reduced back to the progenitor enamine **I**, as corroborated by the irreversible cyclic voltammogram of the preformed enamine **4** (Figure S16 in the SI). Instead, the α-iminyl radical cation **V** collapses to give a variety of degradation products that, despite our efforts, have remained unidentified so far. Thus, the enamine **I** serves as a sacrificial initiator of the chain mechanism[35] since, for any photoinduced SET event, a propagating radical **IV** is generated while a molecule of the chiral catalyst **A** is destroyed via decomposition of the intermediate **V**. By using both gas chromatography (GC-FID) and NMR analyses,[36] we established that the amount of catalyst **A** decreases constantly during the photochemical alkylation in correlation with the number of initiation events (further discussions in the following sections).

With a clearer mechanistic picture in mind, we decided to perform kinetic studies to better understand the relative importance of the initiation step and the propagation cycle for the overall rate, while establishing the rate-determining step of the model photochemical alkylations. But before this, we investigated whether the different photochemical pathways available to enamines for initiating the chain process (EDA complex formation vs direct photoexcitation) might have an influence on the enamine formation and its concentration in solution. This matters because the amount of enamine in solution has a direct effect on the kinetic profiles of the reactions, since the enamine is involved in both initiation and chain propagation.

NMR Spectroscopic Studies. The catalytically active enamine intermediate **I** is generated via the reversible condensation of the chiral aminocatalyst **A** with butanal **1a** (Figure 8a). This reversible process is characterized by an equilibrium constant ($K_{enamine}$). As with all chemical equilibria, the system follows Le Châtelier's principle. As a consequence, any perturbation of the equilibrium (as induced by a change in concentration, for example) will shift the position of equilibrium to the side that opposes the perturbation. As discussed above (Figure 3c), the formation of the enamine-based EDA complex is also an equilibrium, where K_{EDA} identifies the association constant. For example, the EDA complex **IIa** (formed by the association of the preformed enamine **4** with 2,4-dinitrobenzyl bromide **2a**) has a K_{EDA} of 11.6 M^{-1} in MTBE. This scenario suggests that the presence of acceptor **2a** can alter the original state of equilibrium for enamine formation. In other words, it can directly influence the relative concentration of free catalyst **A** and enamine **I** in solution (Figure 8a).

To verify this possibility, we used ^{1}H NMR spectroscopic analysis to investigate the equilibrium of enamine formation under the reaction conditions (Figure 8b). Upon mixing 0.3 mmol of **1a** and 0.02 mmol of the aminocatalyst **A** in 0.5 mL of CD_3CN, both enamine **I** and free catalyst **A** were detected in a ratio of 1.2:1. An equilibrium constant ($K_{enamine}$) of 1.9±0.2 M^{-1} was determined. The addition of 0.1 mmol of **2a** induced a shift in the position of the equilibrium toward the enamine **I**, as demonstrated by the 1.8:1 ratio of **I** and free catalyst **A**. This is congruent with the fact that the formation of the EDA complex, by sequestering **I**, shifts the dynamic equilibrium of enamine formation to the side that reduces the perturbation (in this case, the forward reaction).[37] Since these studies were made in the absence of light, we then studied the effect of illumination on the dynamic equilibrium system (Figure 8c). We used a xenon lamp coupled with a monochromator which, by bringing the light in close contact with the NMR tube through an optical fiber,[38] allowed for the *in situ* illumination of the samples. When the EDA complex mixture, originally kept in the dark, was irradiated *in situ* in the NMR spectrometer (λ = 470±5 nm, irradiance = 28.8 μW/cm^2), a large shift in the position of the enamine equilibrium was immediately observed (3.8:1 ratio of **I**:**A** after 30 seconds of irradiation). After 60 seconds of irradiation, the signals of the free catalyst **A** could no longer be detected, meaning that the system dramatically shifted towards the enamine **I**. This observation can be reconciled with the photochemical activity of the enamine-based EDA complex **II**, which, upon excitation, induces the *irreversible* formation of the electrophilic radical **IV** (upon fragmentation of the C-Br bond within the ion pair **III**, see Figure 3d) and the unstable α-iminyl radical cation **V**.[36] These light-triggered events decrease the concentration of both the enamine and **2a**, further favoring the

forward reactions of the multiple equilibrium systems depicted in Figure 8c.

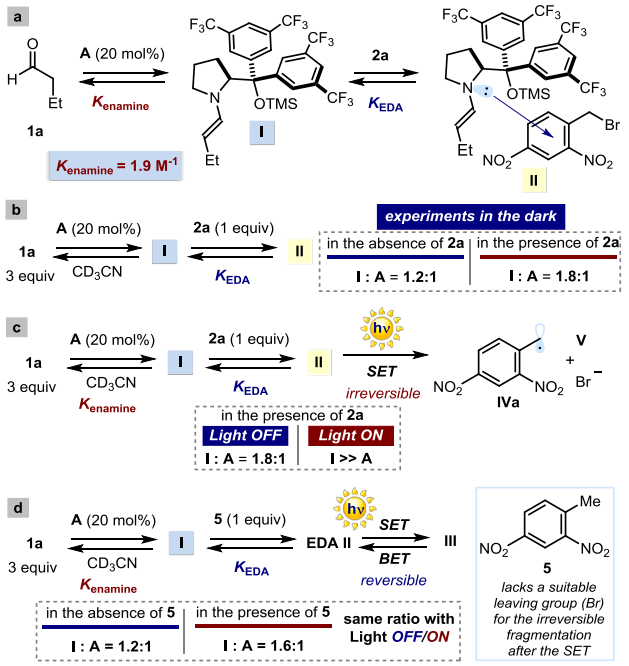

Figure 8. Influence of the EDA complex formation on the amount of enamine in solution. ^{1}H NMR experiments were performed in CD_3CN at 298 K using a xenon lamp coupled with a monochromator and equipped with an optical fiber for the *in situ* illumination of the samples (λ = 470±5 nm, irradiance = 28.8 μW/cm^2). (**a**) The equilibrium constant for the enamine **I** formation ($K_{enamine}$) and the following equilibrium to form an EDA complex **II** with **2a** (K_{EDA}); (**b**) effect on the position of equilibrium for enamine formation in the absence and the presence of the EDA acceptor **2a**. (**c**) The effect of light illumination and the irreversible step (triggered by the photoactivity of the EDA complex **II**) on the concentration of enamine in solution (see Figure 3d for more details and the structures of intermediates **III** and **V**). (**d**) The effect of an EDA complex, unable to undergo a photoinduced irreversible SET event, on the enamine concentration. BET: back electron transfer.

The importance of the irreversible events that follow the photoinduced SET is corroborated by a similar experiment where **2a** was replaced by 2,4-dinitrotoluene **5** (Figure 8d). **5** can act as an acceptor partner in EDA complex formation with the enamine **I** (K_{EDA} = 4.6 ± 0.1 M^{-1} in MTBE with enamine **4**), but it cannot undergo an irreversible fragmentation, since it lacks a suitable leaving group (e.g. the bromine within **2a**). In the dark, the addition of 1 equiv of **5** to a solution of catalyst **A** and butanal **1a** induced a displacement in the equilibrium of the enamine formation, changing the **I**:**A** ratio from 1.2:1 to 1.6:1. This is because an EDA complex **II** can be generated, which perturbs the equilibrium of enamine formation. In sharp contrast, illumination did not change the concentration of the enamine **I** to any extent. This observation is consonant with an unproductive photoinduced SET and a fast back electron transfer (BET) that, by restoring the ground state EDA complex **II**, do not influence either the overall equilibrium of the system or the distribution of catalyst **A**, which is partitioned between the free state and the enamine **I**.

These experiments were then repeated with the bromomalonate **2c** (results not shown in Figure 8). In this case, the equilibrium of the enamine formation ($K_{enamine}$= 1.9 M^{-1} as in Figure 8a) was not perturbed by the addition of **2c**. This is because the mechanism of initiation is based on the direct photo-excitation of the enamine **I** and does not involve any pre-association with **2c**. Thus, the presence of **2c** does not influence the partitioning of the catalyst **A** between the free state and the enamine **I**.

Kinetic Studies. We then performed kinetic studies to gain a better understanding of the factors governing the photochemical enamine-based alkylations of butanal **1a**. In particular, we sought to assess whether the existence of two different initiation methods, but seemingly similar propagation cycles, would bring about distinct or analogous kinetic profiles. The amine **A**-catalyzed alkylation of **1a** with 2,4-dinitrobenzyl bromide **2a** was chosen as representative of the EDA complex activation strategy (Figure 9a),[39] while the reaction with diethyl bromomalonate **2c** exploits the direct photoexcitation of the enamine (Figure 9b). Initial rate experiments were performed in acetonitrile as the solvent to avoid the precipitation of the lutidinium bromide, generated during the reaction.[28] The progress of the two reactions was monitored by ^{1}H NMR analysis using two different approaches (see Section I in the SI for details). We used a Xenon lamp with a band-pass filter at 450 nm (irradiance = 4.7 μW/cm^2) to illuminate the EDA complex-mediated reaction with **2a** (Figure 9a), while a cut-off filter at 385 nm (irradiation at λ ≥ 385 nm; irradiance = 300 μW/cm^2) was employed for the process with **2c** (Figure 9b). This set-up required an independent reaction to be performed for every data-point at different times.

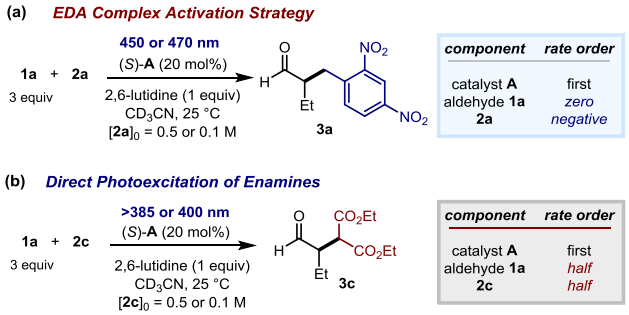

Figure 9. Model reactions used for initial-rate kinetics determined by ^{1}H NMR analysis and the observed rate orders. (**a**) EDA complex-triggered photochemical alkylation of butanal **1a** with 2,4-dinitrobenzyl bromide **2a**. (**b**) Alkylation of **1a** with diethyl bromomalonate **2c** driven by the direct photoexcitation of enamines. Reaction conditions: studies performed across a range of concentrations for each reaction component in CD_3CN, irradiation at 450 and >385 nm for **2a** and **2c**, respectively. The kinetic studies were repeated using *in situ* ^{1}H NMR spectroscopy (λ = 470 and 400 nm for **2a** and **2c**, respectively) to directly monitor the reaction progress. Both approaches gave similar kinetic profiles.

The initial-rate kinetic studies were repeated using *in situ* ^{1}H NMR spectroscopy to directly monitor the reaction progress.[40] In this second case, we used a Xenon lamp coupled with a monochromator which allowed for the *in situ* illumination of the samples. The EDA complex-based reaction with **2a** was irradiated at 470 nm (irradiance = 28.8 μW/cm^2), while

400 nm (irradiance = 20.4 μW/cm^2) was used for the alkylation chemistry with **2c**. Both approaches gave similar and reproducible kinetic profiles.

Figure 9 details the results of our initial-rate kinetic investigations, performed across a range of concentrations for each reaction component.[41] A first-order dependence on the catalyst **A** was inferred for both the EDA complex-based process with **2a** (Figure 9a) and the reaction with bromomalonate **2c** (Figure 9b). However, striking discrepancies in rate orders were observed in the dependence on butanal **1a** and organic halide (**2a** and **2c**). The EDA complex-mediated alkylation showed a zero-order dependence in **1a** concentration and an unexpected *negative* fractional order in [**2a**]. In sharp contrast, the photochemical alkylation of **2c** is characterized by a half-order dependence on both [**1a**] and [**2c**].

We then tried to reconcile the strikingly different kinetic behaviors of the two systems with our previous observations. The zero-order dependence on butanal **1a** for the EDA complex-mediated alkylation with **2a** implies that the enamine **I**, generated *in situ* upon condensation of **A** and **1a**, is the resting state of catalyst **A**. This conclusion is consonant with the NMR spectroscopic studies reported in Figures 8b-c indicating that, under the reaction conditions - that is, when the EDA complex between the enamine **I** and **2a** is formed and under illumination - the equilibrium position of the enamine formation is completely shifted toward the enamine **I**. This means that a negligible amount of catalyst **A** is available in its free state and, consequently, the concentration of **1a** does not affect the formation of the reactive enamine catalytic intermediate. In sharp contrast, our NMR studies established that the equilibrium of the enamine formation is not perturbed by the addition of bromomalonate **2c**. In the direct photoexcitation of the enamine **I**, the amine catalyst **A** is partitioned between the free state and the enamine intermediate **I**. Thus, a definitive resting state cannot be identified, with the catalyst concentration shared between different intermediates. This situation is congruent with the observed positive fractional order in [**1a**] (Figure 9b).

Concerning the reaction rate's dependence on the alkyl halide **2**, the negative fractional order in [**2a**] for the EDA complex-driven process (Figure 10a) deserves in-depth discussion. As previously mentioned, for any SET event taking place within the photoactive EDA complex (Figure 3d and initiation step in Figure 7), a propagating radical **IV** is generated while a molecule of the chiral catalyst **A** is destroyed via decomposition of the unstable α-iminyl radical cation **V**.[36] To verify whether the disappearance of the catalyst was related to the number of initiation events, we followed the evolution of [**A**] over time across a range of concentrations of **2a**, which is the acceptor partner in EDA complex formation. Since there is zero-order dependence in [**1a**] and due to the fact that we could not detect any trace of catalyst **A** in its free state by NMR analysis, we monitored the evolution of **A** in our experiments by determining the enamine concentration in solution.[37] The initial-rate measurements in Figure 10b suggest that the decrease in [**A**] correlates with **2a** concentration. If the rate of disappearance of [**A**] is proportional to [**2a**]^n, then the data should fit Equation 1. As a result, the kinetic data can be plotted as indicated in Equation 2.

$$\text{Disappearance of } \mathbf{A} = -\mathrm{d}[\mathbf{A}]/\mathrm{d}t \propto [\mathbf{2a}]^n \quad \text{(Eq. 1)}$$

$$[\mathbf{A}] \propto [\mathbf{2a}]^n \cdot t \quad \text{(Eq. 2)}$$

Equation 2 indicates that, for reactions with the same initial concentrations of aminocatalyst **A**, plots of [**A**] versus [**2a**]$^n \cdot t$ should be superimposable.[42] Figure 10c shows such a superimposition for three reactions that have comparable initial concentrations of **A** but different concentrations of **2a**. In Figure 10c, the overlay found for plots of [**A**] versus [**2a**]$^1 \cdot t$ (n = 1 in Equation 2) establishes a first-order dependence on [**2a**] for the catalyst's disappearance.

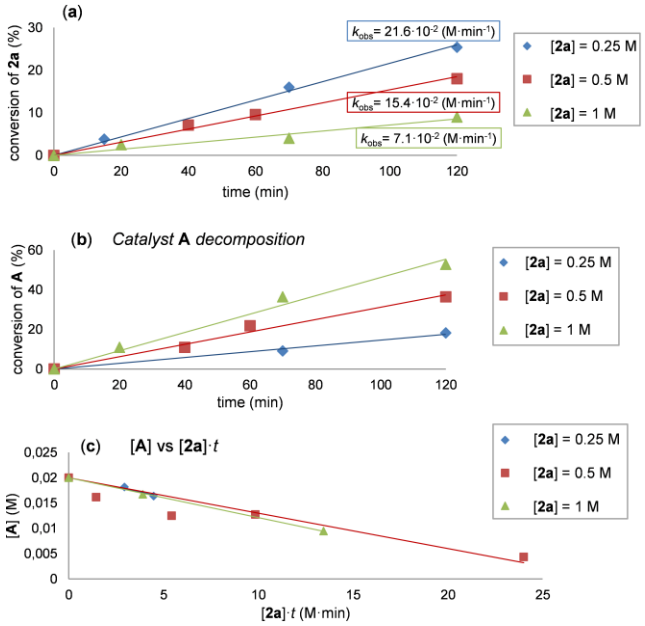

Figure 10. (**a**) Reaction profiles for different [**2a**] showing a negative-order dependence and observed rate constants. K_{obs} calculated from the slope of the plots. (**b**) Evolution of the catalyst concentration for the experiments in Figure 10a. We monitored the evolution of **A** by determining the enamine concentration in solution. (**c**) Overlay of plots for the kinetic data in Figure 10b according to Equation 2. Progress of the reactions followed by ^{1}H NMR analysis; each point corresponds to an individual run. Reactions performed in CD_3CN under illumination by a Xenon lamp with a band-pass filter at 450 nm (irradiance = 4.7 μW/cm^2); [**1a**]$_0$= 1.5 M, [**A**]$_0$= 0.1 M; initial concentrations of **2a**: 0.25 M (blue plot); 0.5 M (red plot) and 1 M (green plot). The same kinetic profiles have been observed using *in situ* NMR monitoring of the reaction progress, see Section I1 in the SI.

The unitary dependence was also observed using *in situ* NMR monitoring of the reaction progress (see Sections F3 and I1 in the SI for details). Using this approach, we performed two sets of experiments under the same conditions, but using a different intensity of irradiation (λ = 470 nm for both sets of experiments, but irradiance = 28.8 vs 3.0 μW/cm^2). In the latter set of experiments, a lower absolute rate of catalyst decomposition was determined, in consonance with a less effective initiation regime. This observation establishes a direct correlation between the disappearance of catalyst **A** and the number of photochemical initiation events, since both the concentration of **2a** and the intensity of light influence the rate of degradation for catalyst **A**.

We then wanted to measure the real effect of [**2a**] on the rate of alkylation leading to product **3a**, discounting the effects of catalyst **A** degradation in the initiation regime. Considering the zero-order dependence on **1a**, the rate equation should read as Equation 3, with *n* being the rate order with respect to **2a**, overlooking its effect on [**A**].

$$\text{Reaction rate} = d[\mathbf{3a}]/dt \propto [\mathbf{A}]^1 \cdot [\mathbf{2a}]^n \quad \text{(Eq. 3)}$$

$$[\mathbf{3a}]/[\mathbf{A}] \propto [\mathbf{2a}]^n \cdot t \quad \text{(Eq. 4)}$$

Figure 11 shows the plotting of the kinetic data as indicated in Equation 4, which is readily derived from Equation 3. In Equation 4, the product formation is normalized by [**A**], thus discounting the effect of the catalyst degradation. There is significantly better overlay for plots of $[\mathbf{3a}]\cdot[\mathbf{A}]^{-1}$ vs $[\mathbf{2a}]^{0.2}\cdot t$ (n = 0.2 in Equation 4) than for plots of $[\mathbf{3a}]\cdot[\mathbf{A}]^{-1}$ vs t or $[\mathbf{3a}]\cdot[\mathbf{A}]^{-1}$ vs $[\mathbf{2a}]^1\cdot t$ (n = 0 and 1, respectively). This indicates a *positive* fractional-order dependence on [**2a**] (n ≈ 0.2, line of best fit).

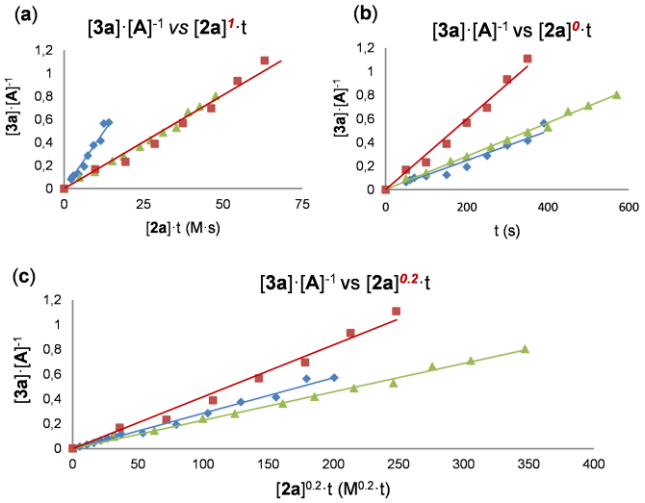

Figure 11. Plots of the kinetic data according to Equation 4 for different values of *n*: (**a**) *n* = 1, (**b**) *n* = 0, and (**c**) *n* = 0.2. The plots should be superimposable for the value of *n* that better renders the reaction order with respect to **2a**. For this fitting, we have used the data obtained by *in situ* NMR monitoring of the reaction progress which gives the same kinetic profiles observed in Figure 10 (Section I1 in the SI). This approach has the advantage to provide a larger number of data, thus allowing for a more reliable fitting. Experiments performed in NMR tubes at 298 K in CD_3CN using a monochromatic light (λ = 470 nm, irradiance 28.8 μW/cm^2); $[\mathbf{1a}]_0$= 0.3 M, $[\mathbf{A}]_0$= 0.02 M; initial concentrations of **2a**: 0.05 M (blue plot); 0.1 M (red plot) and 0.2 M (green plot).

Overall, Equation 5 gives the empirical rate low for the EDA complex-mediated alkylation of butanal in Figure 9a, discounting catalyst degradation related to the photochemical initiation:

$$\text{rate} = d[\mathbf{3a}]/dt = k\,[\mathbf{A}]^1 \cdot [\mathbf{2a}]^{\approx 0.2} \quad \text{(Eq. 5)}$$

The rate low indicates a rate-determining step within the radical chain propagation cycle (see Figure 7 for the general mechanism). If the initiation step was rate-limiting, a first-order dependence with respect to both EDA partners **I** and **2a** would be expected instead. The first-order dependence on catalyst **A** (whose concentration is equal to the enamine **I** concentration) suggests that the rate-determining step is the trapping of the electrophilic carbon-centered radical **IV** from the ground state chiral enamine **I** to form the new carbon-carbon bond. We would expect higher-order dependence in [**2a**] if the rate-limiting step were the SET process, which regenerates the chain-propagating radical **IV** from the α-aminoalkyl radicals **VI**.

The alkylation of **1a** with bromomalonate, driven by the direct excitation of enamine, shows half-order dependence in [**2c**]. The overall rate equation is then given by Equation 6:

$$\text{rate} = d[\mathbf{3c}]/dt = k\,[\mathbf{A}]^1 \cdot [\mathbf{1a}]^{0.5} \cdot [\mathbf{2c}]^{0.5} \quad \text{(Eq. 6)}$$

In analogy with the preceding discussion, the rate-order assessment indicates that the rate-determining step is the enamine trapping the electrophilic radical **IV**, derived from **2c**, to form the carbon-carbon bond (see Figure 7 for the general mechanism).

Notable, no significant degradation of catalyst **A** was observed during the alkylation with **2c** within the timeframe of interest for the initial-rate measurements using the method of independent experiments.[43] When extending the time of irradiation of the photochemical alkylation with **2c**, the disappearance of catalyst **A** became significant. However, using the same 23 W CFL light source and considering the same time interval, the catalyst degradation was much higher in the alkylations of **2a** and **2b** than **2c** (details in Section F of the SI). This suggests that the direct excitation of the enamine **I** is a less effective radical generation strategy than the enamine-based EDA complex approach.[44] This scenario can be rationalized on the basis of the bimolecular nature of the initiation mechanism with **2c**, which requires the excited enamine to encounter **2c** for an effective SET. These conditions make an unproductive relaxation of the excited intermediate, which restores the ground state enamine, more likely. In contrast, the photochemistry underlying the processes with **2a** and **2b** is dominated by EDA complexes. These form in the ground state, holding together the two partners involved in the following photo-induced SET. In this case, the initiation mechanism is based on a more efficient unimolecular process.

CONCLUSIONS

In summary, we have used a combination of conventional photophysical investigations, NMR spectroscopy, and kinetic studies to elucidate the key mechanistic aspects of the enantioselective photochemical α-alkylation of aldehydes with electron-poor organic halides. Quantum yield measurements established that a radical chain propagation mechanism is operative, while reaction profile analysis and rate-order assessment indicated that the trapping of the carbon-centered radical by the enamine is the rate-determining event. Central to these processes is the unique and diverse reactivity of chiral enamines. Their photochemical activity, either by EDA complex activation or direct excitation, generates radicals from the organic halides **2a-c**. This event, by feeding in radicals from outside the chain, serves as the initiation of self-propagating cycles.

The enamine lies at the heart of the propagation cycle too, since it traps the radical to generate an intermediate (the α-amino radical **VI**) which is key for sustaining the chain sequence. We also uncovered how enamine formation and its concentration in solution are directly influenced by the different photochemical pathways available to enamines for initiating the chain process (EDA complex formation vs direct photoexcitation). Overall, the kinetic and spectroscopic investigations allowed us to understand the delicate interplay between the light-triggered initiation step and the radical propagation manifold, suggesting that this approach can be generally applied to the mechanistic elucidation of chain processes. From a broader perspective, this study demonstrates that the synthetic potential of chiral enamines is not limited to the ground state domain, but can be further expanded by exploiting their photochemical activity, providing novel reactivity frameworks for conceiving light-driven enantioselective catalytic processes.

ASSOCIATED CONTENT

Complete experimental procedures, characterization data, and details on kinetic and spectroscopic studies. This material is available free of charge via the Internet at http://pubs.acs.org.

Corresponding Author

pmelchiorre@iciq.es

ACKNOWLEDGMENT

Financial support was provided by the ICIQ Foundation, MINECO (project CTQ2013-45938-P and Severo Ochoa Excellence Accreditation 2014-2018, SEV-2013-0319), the AGAUR (2014 SGR 1059), and the European Research Council (ERC 278541 - ORGA-NAUT). A.B. is grateful to the MECD for a FPU fellowship (Ref. FPU13/02402). The authors thank Dr Elena Arceo and Dr Mattia Silvi for preliminary investigations and useful discussions.

REFERENCES

(1) (a) Stork, G.; Terrell, R.; Szmuszkovicz, J. *J. Am. Chem. Soc.* **1954**, *76*, 2029–2030. (b) Stork, G.; Brizzolara, A.; Landesman, H.; Szmuszkovicz, J.; Terrell, R. *J. Am. Chem. Soc.* **1963**, *85*, 207–222.

(2) For seminal papers, see: (a) Eder, U.; Sauer, G.; Wiechert, R. *Angew. Chem., Int. Ed. Engl.* **1971**, *10*, 496–497; (b) Hajos, Z. G.; Parrish, D. R. *J. Org. Chem.* **1974**, *39*, 1615–1621. (c) List, B.; Lerner, R. A.; Barbas III, C. F. *J. Am. Chem. Soc.* **2000**, *122*, 2395–2396.

(3) For insightful perspectives on the scientific roots of enamine-mediated stereoselective catalytic reactions, see: (a) Barbas III, C. F. *Angew. Chem., Int. Ed.* **2008**, *47*, 42–47. (b) List, B. *Angew. Chem., Int. Ed.* **2010**, *49*, 1730–1734.

(4) Mukherjee, S.; Yang, J. W.; Hoffmann, S.; List, B. *Chem. Rev.* **2007**, *107*, 5471–5569.

(5) (a) Arceo, E.; Jurberg, I. D.; Álvarez-Fernández, A.; Melchiorre, P. *Nature Chem.* **2013**, *5*, 750–756. (b) Arceo, E.; Bahamonde, A.; Bergonzini, G.; Melchiorre, P. *Chem. Sci.* **2014**, *5*, 2438–2442. (c) Silvi, M.; Arceo, E.; Jurberg, I. D.; Cassani, C.; Melchiorre, P. *J. Am. Chem. Soc.* **2015**, *137*, 6120–6123.

(6) Prior to our studies, similar enamine-mediated enantioselective alkylations of aldehydes were realized using an external photoredox catalyst, which served to generate the radical species from alkyl halides, see: (a) Nicewicz, D. A.; MacMillan, D. W. C. *Science* **2008**, *322*, 77–80. (b) Shih, H.-W.; Vander Wal, M. N.; Grange, R. L.; MacMillan, D. W. C. *J. Am. Chem. Soc.* **2010**, *132*, 13600–13603.

(7) For reviews, see: (a) Foster, R. *J. Phys. Chem.* **1980**, *84*, 2135–2141. (b) Rosokha, S. V.; Kochi, J. K. *Acc. Chem. Res.* **2008**, *41*, 641–653. For the seminal studies that inspired the EDA complex theory, see: (c) Mulliken, R. S. *J. Phys. Chem.* **1952**, *56*, 801–822. (d) H. A. Benesi, J. J. Hildebrand, *J. Am. Chem. Soc.* **1949**, *71*, 2703–2707. (e) R. S. Mulliken, *J. Am. Chem. Soc.* **1950**, *72*, 600–608. (f) R. M. Keefer, L. J. Andrews, *J. Am. Chem. Soc.* **1950**, *72*, 4677–4681.

(8) For the use of chiral enolates, generated under phase-transfer conditions, to form chiral photoactive EDA complexes while promoting an enantioselective process, see: Woźniak, Ł.; Murphy, J. J.; Melchiorre, P. *J. Am. Chem. Soc.* **2015***, 137*, 5678–5681.

(9) Despite their synthetic potential, it is challenging to develop enantioselective catalytic variants of visible light-driven photochemical reactions. For recent reviews discussing the available strategies, see: (a) Brimioulle, R.; Lenhart, D.; Maturi, M. M.; Bach, T. *Angew. Chem., Int. Ed.* **2015**, *54*, 3872–3890. (b) Meggers, E. *Chem. Commun.* **2015**, *51*, 3290–3301. For selected examples, see: (c) Bauer, A.; Westkamper, F.; Grimme, S.; Bach, T. *Nature* **2005**, *436*, 1139–1140. (d) Brimioulle, R.; Bach, T. *Science* **2013**, *342*, 840–843. (e) Alonso, R.; Bach, T. *Angew. Chem., Int. Ed.* **2014**, *53*, 4368–4371. (f) Du, J.; Skubi, K. L.; Schultz, D. M.; Yoon, T. P. *Science* **2014**, *344*, 392–396. (g) Huo, H.; Shen, X.; Wang, C.; Zhang, L.; Röse, P.; Chen, L.-A.; Harms, K.; Marsch, M.; Hilt, G.; Meggers, E. *Nature* **2014**, *515*, 100–103. (h) Kainz, Q. M.; Matier, C. D.; Bartoszewicz, A.; Zultanski, S. L.; Peters, J. C.; Fu, G. C. *Science* **2016,** *351*, 681–684.

(10) For a recent review, see: Donslund, B. S.; Johansen, T. K.; Poulsen, P. H.; Halskov, K. S.; Jørgensen, K. A. *Angew. Chem., Int. Ed.* **2015**, *54*, 13860–13874.

(11) The reactions required the presence of 1 equiv of a base (2,6-lutidine and NaOAc giving similar results) to perform well. Removing the base additive, trace amounts of the alkylation products **3** were formed (<15%), while reagent decomposition along with acidification of the reaction medium was observed. The likely role of 2,6-lutidine is to quench the acid generated during the process, as testified to by the formation of the insoluble lutidinium bromide salt generated during the reaction. The presence of 2,6-lutidine does not contribute to the absorption in the visible region to any extent.

(12) Performing the alkylation with **2c** under the conditions set out in Figure 2c but in the presence of 0.5 mol% of $Ru(bpy)_3^{2+}$ as an external photosensitizer significantly increased the reactivity (two-fold reaction rate), in consonance with the occurrence of an additional photoinduced electron transfer pathway, see Ref. 6a. The increase in reactivity becomes larger in polar solvents (DMF, CH_3CN), where $Ru(bpy)_3^{2+}$ is completely soluble. Details are reported in the Supporting Information of Ref. 5c.

(13) Enamines have a low ionization potential; for example 1-(but-1-enyl)pyrrolidine has an IP of 7.2 eV, see: Müller, K.; Previdoli, F.; Desilvestro, H. *Helv. Chim. Acta* **1981**, *64***,** 2497–2507.

(14) The electron-donor property of a donor molecule is indicated by the magnitude of its ionization potential (*IP* in the gas phase) or its oxidation potential (E_p^{ox} in solution). Conversely, the viability of a compound as an acceptor is indicated by the magnitude of its electron affinity (*EA* in the gas phase) or its reduction potential (E_p^{red} in solution). E_p^{ox} and E_p^{red}, which can be estimated by cyclic voltammetry measurements, can help in predicting the suitability of a given substrate to undergo EDA complex formation.

(15) According to the Mulliken theory (Ref. 7c), the charge-transfer transition energy ($h\nu_{CT}$) is given by the following equation: $h\nu_{CT} = IP - EA - \omega$, where ω is the electrostatic interactions of the charge-transfer ion pair (e.g. **III** in Figure 3d). Qualitatively, the equation predicts that the charge-transfer band of the EDA complexes with a given electron donor (in this case, the enamine) undergoes bathochromic shift (absorption at longer wavelengths) with increasing *EA* of the acceptor component. The same effect can be obtained by increasing the electron donicity (decreasing the *IP*) of the donor.

(16) 2-Phenylacetaldehyde is a competent substrate of the photo-organocatalytic reaction with **2a, 2b**, and **2c**, providing full conversion into the corresponding products under the conditions set out in Figure 2. However, a low level of enantioselectivity was observed (below 30% ee), a consequence of the lability of the resulting benzylic stereocenter.
(17) Job, P. *Ann. Chem.* **1928**, *9*, 113−203.
(18) Benesi, H.; Hildebrand, J. *J. Am. Chem. Soc.* 1949, **71**, 2703−2707.
(19) Costentin, C.; Robert, M.; Savéant, J.-M. *Chem. Physics* **2006**, *324*, 40–56.
(20) Although the photophysics of EDA complexes have been extensively studied (Refs 7a-b), their use in chemical synthesis has found limited applications. This is mainly because the unproductive, back electron transfer (BET), which restores the ground state EDA complex, is generally faster than other possible processes leading to products. For a pertinent discussion, see: Rathore, R.; Kochi, J. K. *Advances Phys. Org. Chem.* **2000**, *35***,** 193–318.
(21) For an additional example of an enamine, formed upon condensation of an aliphatic aldehyde and a secondary amine, which weakly absorbs in the visible region, see: González-Béjar, M.; Peters, K.; Hallett-Tapley, G. L.; Grenier, M.; Scaiano, J. C. *Chem. Commun.* **2013**, *49*, 1732–1734.
(22) For examples of photoinduced reductive cleavage of C-X bonds in electron-poor alkyl halides via a SET from excited substrates, see: (a) Rico, I.; Cantacuzene D.; Wakselman, C. *Tetrahedron Lett.* **1981**, *22*, 3405–3408. (b) Iwasaki, T.; Sawada, T.; Okuyama, M.; Kamada, H. *J. Phys. Chem.* **1978**, *82*, 371–372. (c) Barata-Vallejo, S.; Flesia, M. M.; Lantaño, B.; Argüello, J. E.; Peñéñory, A. B.; Postigo, A. *Eur. J. Org. Chem.* **2013**, 998–1008.
(23) An electronically excited state possesses a much lower ionization potential (i.e. it is a better reductant) than the ground state, see: Turro, N. J.; Ramamurthy, V.; Scaiano, J. C. "Energy transfer and electron transfer" in *Modern molecular photochemistry of organic molecules*, University Science Books, 2010; chapter 7, pp 383. Since an excited state has an inherent propensity to form a supramolecular complex, the generation of an exciplex between the excited enamine **I*** and bromomalonate **2c** cannot be excluded; however, we could not observe any emission diagnostic of possible excited state aggregations.
(24) (a) Studer, A.; Curran, D. P. *Angew. Chem., Int. Ed.* **2016**, *55*, 58–102. (b) Kärkäs, M. D.; Matsuura, B. S.; Stephenson, C. R. J. *Science* **2015**, *349*, 1285–1286.
(25) (a) Ismaili, H.; Pitre, S. P.; Scaiano, J. C. *Catal. Sci. Technol.* **2013**, *3*, 935–937. (b) Wayner, D. D. M.; Dannenberg, J. J.; Griller, D. *Chem. Phys. Lett.* **1986**, *131*, 189–191.
(26) Julliard, M.; Chanon, M. *Chem. Rev.* **1983**, *83*, 425–506.
(27) For a process in which one photon produces only one molecule of the product, the quantum yield can be maximum 1, while for a chain process where one photon forms *n* molecules of product, the quantum yield is expected to be > 1. But a value of $\Phi < 1$ does not exclude a possible radical chain mechanism. This is because of potential non-productive energy wasting photochemical processes.
(28) Both the quantum yield measurements and the kinetic experiments were performed in acetonitrile to avoid the precipitation of the lutidinium bromide salt generated during the reaction (see Ref. 11), which is insoluble in MTBE instead. The presence of a precipitate would scatter the irradiating light thus precluding a reliable measurement.
(29) Yoon recently reported that a related enamine-mediated alkylation of octanal with bromomalonate **2c** using a polypyridyl ruthenium(II) complex as an external photoredox catalyst possesses a similar quantum yield ($\Phi = 18$), further indicating a radical chain mechanism, see: Cismesia, M. A.; Yoon, T. P. *Chem. Sci.* **2015**, *6*, 5426–5434.
(30) The two photochemical initiation manifolds can be both operative in the alkylations of butanal with **2a** and **2b**, but only when using a light that can be absorbed by the transiently generated enamine **I** ($\lambda < 415$ nm). Both kinetic experiments and quantum yield measurements with **2a** and **2b** have been conducted using higher wavelengths of irradiation, so to avoid any possible contribution from the direct photoexcitation of enamines. Under these conditions, only the EDA complex activation is a viable strategy to generate radicals from **2a** and **2b**.
(31) Although we acknowledge the possibility of this alternative pathway, we prefer not to draw the α-bromo amine adduct, since we failed to collect any evidence supporting the existence of this fleeting intermediate. Similar atom-transfer mechanisms have been invoked for the alkylation of enol ethers and enamides with electrophilic radicals, see: (a) Curran, D. P.; Ko, S.-B. *Tetrahedron Lett.* **1998**, *39*, 6629–6632. (b) Friestad, G. K.; Wu, Y. *Org. Lett.* **2009**, *11*, 819–822. This pathway was also proposed in Ref. 24a, page 80.
(32) (a) Kornblum, N. *Angew. Chem., Int. Ed. Engl.* **1975**, *14*, 734–745. (b) Rossi, R. A., Pierini, A. B., Peñéñory, A. B. *Chem. Rev.* **2003**, *103***,** 71–168.
(33) Russell, G. A.; Wang, K. *J. Org. Chem.* **1991**, *56***,** 3475–3479.
(34) Russell, G, A.; Ros, F. *J. Am. Chem. Soc.* **1985**, *107***,** 2506–2511.
(35) Interestingly, an analogous sacrificial role of the enamine was proposed to support the mechanism of the alkylation of aldehydes with bromomalonate **2c**, using a dual photoredox-organocatalytic system, see Ref. 6a.
(36) By using an internal standard and *in situ* NMR spectroscopic analysis, we confirmed that the overall amount of the catalyst **A** decreased over time, further supporting the instability of the intermediate **V** generated upon photoinduced SET. Studies on the disappearance of the catalyst are reported in Figure 10. The same studies were repeated using gas chromatography (GC-FID); details are reported in Section F within the SI.
(37) ^{1}H NMR spectroscopic analysis did not allow us to discriminate between the free enamine **I** and the enamine which engages in EDA complex formation with **2a**. The reported **I** to **A** ratio refers to the total amount of enamine **I** present in solution.
(38) For the description and use of a similar illuminating device, based on LED, see: (a) Feldmeier, C.; Bartling, H.; Riedle, E.; Gschwind, R. M. *J. Magn. Res.* **2013**, *232*, 39–44. (b) Feldmeier, C.; Bartling, H.; Magerl, K.; Gschwind, R. M. *Angew. Chem., Int. Ed.* **2015**, *54*, 1347–1351.
(39) Initial-rate kinetic studies on the alkylation of **1a** with phenacyl bromide **2b** gave a very similar profile to the alkylation with **2a** (Figure 9a).This is consistent with the EDA complex activation being the underlying photochemical initiation for both systems. Kinetic studies for the reaction with **2b** are detailed in Section I2 of the SI.
(40) We could not use the method of reaction progress kinetic analysis to provide a rapid and comprehensive kinetic profile of the reactions because of the significant catalyst degradation pathway. For an overview highlighting the potential of this approach, see: Blackmond D. G. *Angew. Chem., Int. Ed.* **2005**, *44*, 4302–4320.
(41) We also explored the effect of water on the reaction rate of the two processes detailed in Figure 9. No alteration of the kinetic profiles was observed after the addition of either 1 or 10 equivalents of H_2O.
(42) For a similar treatment of kinetic data for a reaction proceeding through a radical chain mechanism, see: Boisvert, L.; Denney, M. C.; Kloek Hanson, S.; Goldberg, K. I. *J. Am. Chem. Soc.* **2009**, *131*, 15802–15814.
(43) When monitoring the progress of the alkylation with **2c** using *in situ* NMR methodology, we did observe catalyst degradation. This is presumably because of decomposition pathways triggered by the presence of oxygen in the system, as *in situ* monitoring did not allow for complete de-oxygenation of the reaction medium.
(44) Given that both the EDA complex-driven alkylation with **2a** and the alkylation of **2c** triggered by the enamine excitation have comparable quantum yields ($\Phi = 25$ and 20, respectively), a different efficiency in the photochemical initiation regime would imply a more effective propagation cycle (that is, a larger radical chain length) for the alkylation with bromomalonate **2c**.

Graphical Abstract